Rheological characterization of microfibrillated cellulose suspension using optical coherence tomography

SANNA HAAVISTO, JUHA SALMELA, ARI JÄSBERG, TAPIO SAARINEN, ANNI KARPPINEN, AND ANTTI KOPONEN

ABSTRACT: Fiber suspensions, such as microfibrillated cellulose, are a challenge for conventional rheometers to measure. This is because rheometers have small flow channel dimensions that can restrict flocculation. Often, questionable assumptions are also made about the fluid behavior in the gap. A pipe rheometer and ultrasound velocity profiling-pressure difference (UVP-PD) concept can be used, by which the real flow behavior is used for the rheological analysis of the bulk properties of the suspension. Unfortunately, the resolution of UVP is too low for studying near-wall phenomena, such as the lubrication layer, that are often very important for understanding the rheology and to upscale the results to industrial flows. To address this problem, we have widened the UVP-PD concept with optical coherence tomography measurements. This enables us to measure the bulk and wall-layer behavior simultaneously. Our results demonstrate the benefits of having direct, detailed measurement of the velocity profile inside the rheometer.

Application: Velocity profiling in the near-wall region can lead to better understanding of the rheology of complex fluids. This information would be invaluable in flow control and numerical simulations of flows of complex fluids, such as microfibrillated cellulose (MFC).

Cellulose fibers generally form an opaque flocculated suspension with high viscosity, even at low mass concentrations. Conventional rheometers often fail to produce reliable information for these suspensions because the dimension of the system (e.g., the gap between walls) is typically very small. In addition, interpretation of the measured data is usually based on an assumed flow behavior of the fluid (e.g., Couette-type flow and no-slip boundary condition) that might not be valid. To address these problems, we previously introduced a laboratory-scale pipe rheometer that can be used for any complex fluid, thus it is especially useful for studying fibrous materials [1]. The rheological characterization in the pipe rheometer is based on the well-established ultrasound velocity profiling (UVP) and pressure difference (PD) concept, which has been widely used to study rheological properties of various model and industrial fluids [2-5].

In the UVP-PD method, the rheological analysis is based on a combination of UVP and PD measurements [6,7]. The real flow behavior based on direct experimental observation can thus be used as the basis for interpreting and analyzing the results from the rheometric measurements – no assumptions of the velocity profile are needed. Moreover, the pipe rheometer enables the use of realistic flow geometries where a suspension can reach its steady state, but collective phenomena such as flocculation are not restricted by the system size.

In the data analysis of the UVP-PD method, the local shear rate $\dot{\gamma}(r)$ at each distance r from the tube wall is obtained directly from the measured velocity profile. The local shear stress is:

$$\tau(r) = \tau_w(1-r/R) \quad (1)$$

where R is the pipe radius and $\tau_w = \Delta p/2RL\pi$ is the shear stress at the pipe wall (here Δp is the pressure loss and L is the pipe length). The local shear viscosity (**Fig. 1a**) is then:

$$\mu(r) = \tau(r)/\dot{\gamma}(r) \quad (2)$$

The yield stress τ_y of the fluid is obtained from the measured velocity profile by using this formula:

$$\tau_y = \tau_w(1-R_0/R) \quad (3)$$

where R_0 is the radial position, estimated from the velocity profiles, at which the fiber plug brakes (**Fig. 1b**) [1].

The flow behavior of fiber suspensions, however, cannot be understood from bulk properties alone. A common phenomenon that occurs in fiber suspension flows is the drag reduction, which refers to a case where the frictional loss in a channel suddenly levels off or even decreases with increasing flow rate (**Fig. 2**) [1]. Qualitatively, the origin of this effect can be traced back to a spontaneous formation of a concentration gradient or a fiber-free lubrication layer near the channel

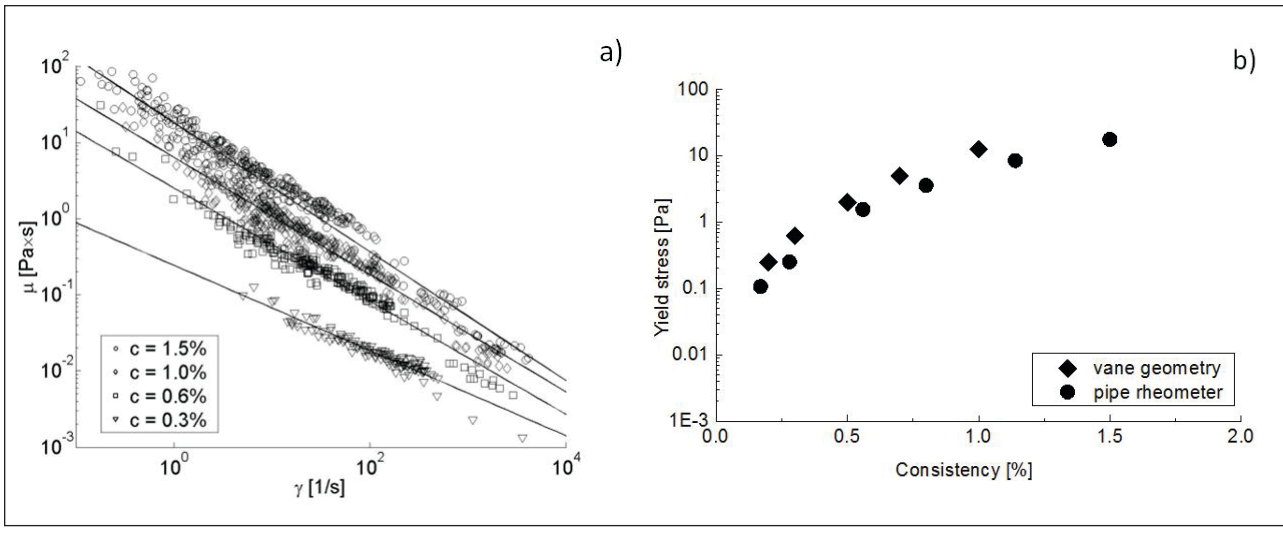

1. (a) Viscosities for different concentrations of microfibrillated cellulose (MFC). The measurements have been performed with the pipe rheometer. (b) Yield stress of a MFC suspension as a function of concentration measured with the pipe rheometer and a rotational rheometer equipped with vane geometry. [1]

wall [8,9]. However, the phenomenon is still poorly understood, posing a problem in flow control and in numerical simulations of fiber suspension flows. Because of its nonlinear behavior, the lubrication layer may create instabilities to the flow. Without accurate knowledge about these dynamics, it is impossible to build control schemes based on physical modeling. The existence of a lubrication layer also affects the results of traditional rheometer measurements, often making them unreliable.

A key reason for developing more reliable material models for fiber suspension flows is to gain more realistic understanding of the boundary layer behavior of such fluids. So far, this has not been feasible because of the lack of experimental techniques that would allow direct measurement of flows and structures of complex, opaque fluids in the immediate vicinity of the wall (typically, within a few tens of micrometers from the wall). Generally, there are very few non-invasive measurement methods available that can be used in measuring the velocity field or the structure of opaque heterogeneous fluids, such as fiber suspensions. Two commonly known methods are magnetic resonance imaging [10] and UVP [11]. More recently, optical coherence tomography (OCT) has been developed and introduced for this purpose [12-14]. OCT is a non-invasive optical imaging technique capable of real-time access of structural data and velocity information in an opaque scattering medium. The most important advantages of OCT as compared to other methods are its high spatial and temporal resolution and its ability to provide reliable data very close to solid boundaries.

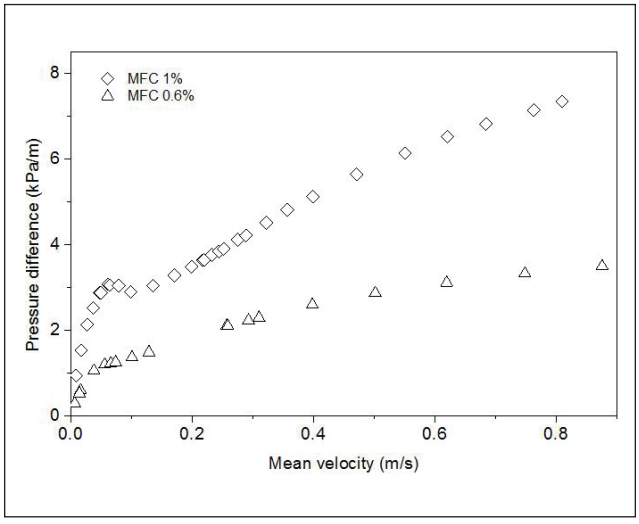

2. Pressure loss as a function of mean velocity for 0.6% MFC and 1.0% MFC. The creation of the lubrication layer (leveling of the pressure loss) is clearly seem for 1.0% MFC at v = 0.1 m/s. The pipe diameter in these experiments was 16 mm. [1]

We have recently equipped the pipe rheometer with the UVP and the OCT techniques [8,15]. This enables the measurement of the whole velocity field in the pipe (including the close wall area). With such a setup, we get all relevant rheological information simultaneously from a single apparatus: bulk properties from UVP and boundary layer behavior from OCT (**Fig. 3**).

Because of some intriguing characteristics of microfibrillated cellulose (MFC) suspensions (e.g., high surface area, high aspect ratio, and ability to form a very rigid network), it has become a considerable part of research in material technology during the past few decades [16]. The rheological properties of MFC suspensions also have been under lively investigation [8,17-20]. In earlier work, we presented indirect evidence of intricate flow phenomena for MFC, such as instability, flocculation, and wall slip inside a rotational rheometer [21,22]. With OCT, we can now take explicit snapshots for the structure of MFC in such a setup. The reported results have

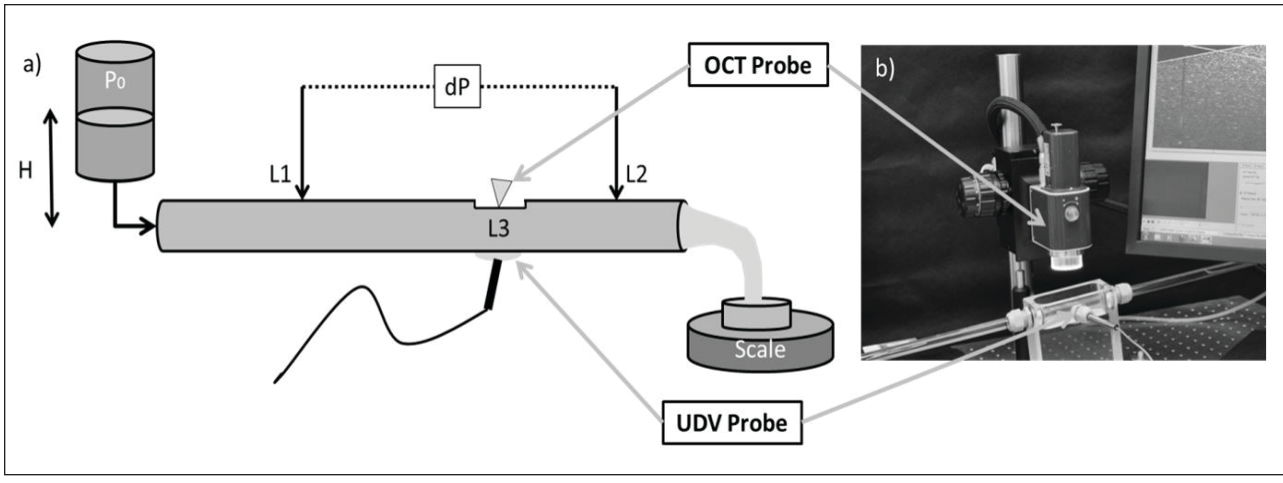

3. (a) Schematic illustration of the measurement setup of the new pipe rheometer. (b) Image of the optical coherence tomography (OCT) measurement setup.

shown strong shear thinning behavior (i.e., a decrease in viscosity with increasing shear rate) for MFC suspensions. We show that the generally used assumption of a stationary nearly linear velocity profile, valid for water and other simple fluids, often is not appropriate here.

MATERIALS AND METHODS

OCT and UVP

The OCT device used in this study was a Spectral Domain OCT (Telesto SD-OCT, Thorlabs; Newton, NJ, USA). In a standard OCT setup, a light beam of low coherence is emitted from a super luminescent LED light source and split into the sample arm and the reference arm of a Michelson interferometer. The backscattered interference pattern can be analyzed for sample scattering index from different depths and further processed to construct slice images from a series of adjacent lateral scans. In Doppler OCT mode, the adjacent scans are used to acquire the velocity information by use of the Kasai autocorrelation function [23]. The resolution and frame rate of the slice images are determined by the light beam properties (central wavelength, coherence length, and dimensions) and the radial/axial scan rate. With the current device, the central wavelength was 1325 nm, radial resolution in water was about 5 μm, and the lateral resolution was 15 μm. Three discrete values, 5.5 kHz, 28 kHz, and 91 kHz, were available for the radial scan rate.

UVP is a method for measuring an instantaneous 1-dimensional velocity profile [11]. The method is based on detecting the Doppler shift frequency information echoed by particles moving with the flow. The actual velocity of the moving particles is calculated from the cross-correlation between the echoes from sequential pulses. The location of the particles is acquired with the time-of-flight method using the known velocity of sound. In the present study, a DOP2000 velocimeter (Signal Processing S.A.; Savigny, Switzerland) equipped with an 8 MHz ultrasound transducer was used. The angle between the transducer axis and the pipe wall was 74°. The ultrasound pulse repetition frequency was varied between 500 Hz and 1000 Hz to exploit the full velocity resolution range. In all measurements, eight consecutive pulse emissions were used to calculate a single velocity value in each sampled depth locations.

Rheological characterization in pipe flow

The measurement unit in the pipe rheometer consists of a 1500 mm long and 8.6 mm inner diameter optical grade glass pipe with 2.5 mm wall thickness. The flow can be driven by gravity or pressurized air to allow for a steady, pulsation-free flow. The mass flow rate is recorded with a laboratory scale and the corresponding pressure loss with pressure difference sensors (Rosemount 3051 and 2051, Emerson Process Management; Shakopee, MN, USA).

The MFC suspension properties were analyzed in similar manner as with UVP alone but now the combined velocity profile (UVP and OCT) was used [1]. The velocity profiles were obtained by a sequence of measurements with increasing flow rate. The region of steady flow was determined from the measurement data and analyzed for average pressure loss and mass flow rate. With UVP and OCT, a set of data was recorded for each flow rate, and the final mean velocity profile was calculated as an average of several instantaneous velocity profiles.

Rheological characterization with rheometer

Stepped flow shear measurements (flow curves) were carried out at room temperature (23°C-25°C) using a dynamic rotational rheometer (AR-G2, TA Instruments; New Castle, DE, USA) equipped with concentric cylinders geometry. We used a standard TA Instruments hard anodized aluminum bob with radius of 14.00 mm and height of 42.00 mm. The outer geometry was a custom-made transparent polymethyl methacrylate (PMMA) cup with radius of 14.87 mm. The flow curves were measured starting from high shear rate (i.e., from 600 to 0.1 s^{-1}) using 15 s point time.

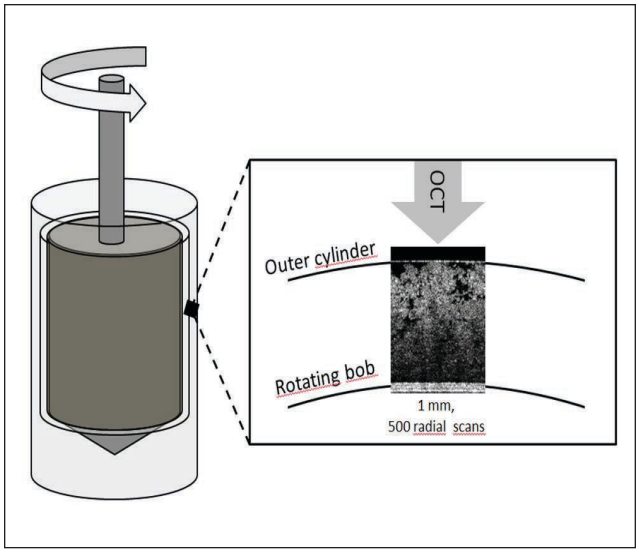

4. Schematic illustration of the concentric cylinder geometry together with the OCT measurement principle.

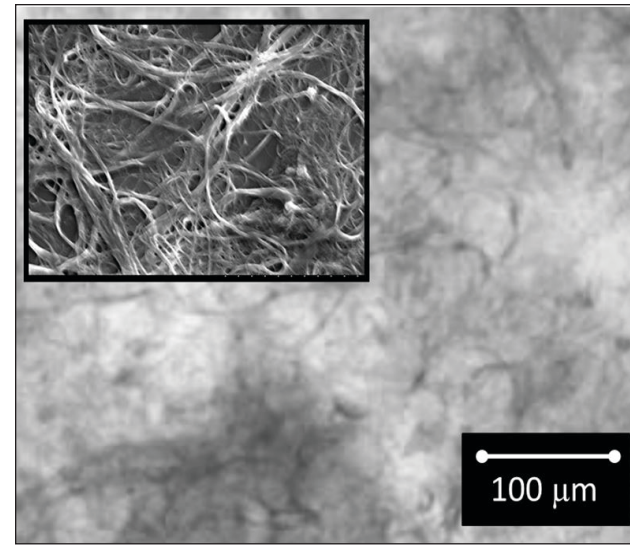

5. Microscopic images of Masuko ground microfibrillated cellulose and Celish KY-100G (upper left corner).

In the stepped flow measurements, OCT was used for imaging the suspension in the radial direction from the transparent outer geometry boundary to the inner geometry boundary (**Fig. 4**). In the higher shear rate range ($\dot{\gamma} > 50$ 1/s), OCT was set to acquire sequential scans from a fixed radial position with the highest available scan rate (i.e., 91 kHz). At the lower shear rates, OCT parameters were selected to allow for detailed visual observation of the MFC suspension structure. A set of 2-dimensional slice images consisting of 500 radial scans across a lateral width of 1 mm were recorded at each shear rate.

Microfibrillated celluloses

The microfibrillated cellulose type used in the pipe rheometer experiments was Celish KY-100G (Daicel Chemical Industries; Himeji, Japan), a commercial product made from purified wood pulp (**Fig. 5**). The average length and diameter of Celish fibers reported by Tatsumi et al. [24] are 350 μm and 15 μm, respectively. The size distribution of the fibrils, however, ranges from microscale to nanoscale. For the experiments, the pulp sample was diluted with deionized water to mass concentrations of 0.4%, 1.0%, and 1.7% under high intensity mixing. The pulp temperature during the measurements was 20±1°C.

The microfibrillated cellulose sample for the rotational rheometer measurements was prepared from bleached kraft birch pulp and ground three times with a supermasscolloider (Masuko Sangyo; Kawaguchi, Japan). Before grinding, the pulp was changed to its sodium form and washed with deionized water until the electrical conductivity was less than 20 μS/cm. The grinding consistency was 1.9%. The sample was diluted with MilliQ water to a mass concentration of 1% and mixed with a propeller mixer for 10 min.

RESULTS

Pipe rheometer

Verification with water

The correct operation of the measurement setup and the consistency of the measured OCT and UVP velocity data were verified with water in laminar and in turbulent flow conditions. This can be done very accurately; the flow of water in a straight smooth tube with circular cross section is well known. **Fig. 6** shows the measured results together with the standard profile correlations [25]. Here, nondimensional wall unit notations for (dimensionless) distance from the pipe wall y^+ and (dimensionless) flow velocity u^+ are used in the following equation:

$$y^+ = \frac{yu^*}{\nu},\ u^+ = \frac{u}{u^*}, u^* = \left(\frac{\tau_w}{\rho}\right)^{\frac{1}{2}} \quad (4)$$

where y is the distance from the wall, ν is the kinematic viscosity of water, u is the fluid velocity, ρ is the fluid density, τ_w is the shear stress at the wall, and u^* is friction velocity.

The results in Fig. 6 show that there is very good agreement between the experimental data and the theoretical prediction in the Reynolds number range of 60–10000 (i.e., flow velocity range of 7×10^{-3} – 1.2 m/s). The profiles measured with both OCT and UVP follow the linear law of the wall ($u^+ = y^+$) and the logarithmic law ($u^+ = \frac{1}{0.40} \ln y^+ + 5.5$) quite accurately. Figure 6 also shows the Spalding profile [26], which smoothly interpolates between the two preceding formulae.

The spatial measurement range of OCT covers the viscous sublayer and part of the buffer layer. It closely follows the theoretical profile over more than two orders of magnitude in y^+. To our knowledge, the data measured with OCT reach smaller values of y^+ (i.e., are measured closer to the wall) than

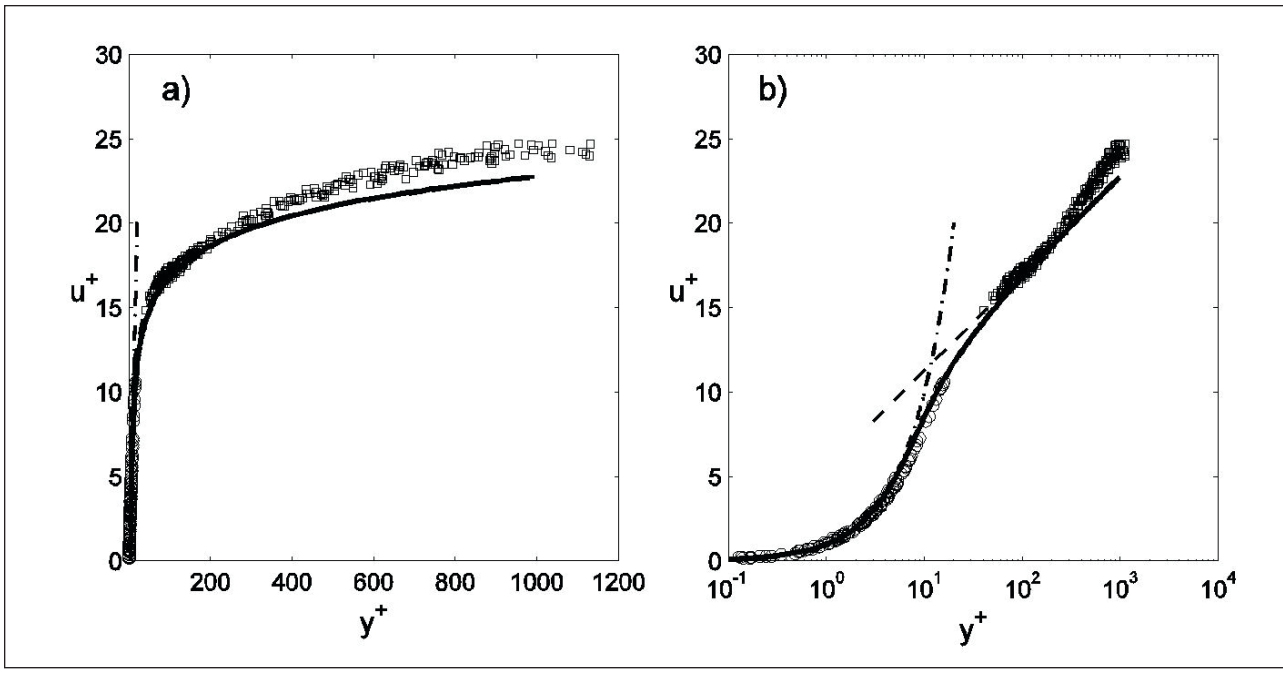

6. Several velocity profiles of laminar and turbulent pipe flows of water measured with OCT (circles) and ultrasound velocity profiling (UVP; squares) in dimensionless variables y^+ and u^+ plotted in (a) linear scales and (b) with logarithmic y^+ scale. The dash-dotted line indicates the linear viscous sublayer profile and the dashed line is the logarithmic buffer layer profile. The solid line represents the Spalding inner layer correlation [26] from which the measured velocity profiles are seen to separate (correctly) at y^+ ~300.

has been reported before for such a small pipe (D = 8.6 mm).

Because the OCT results can be obtained very close to the wall, the shear stress at the wall can be calculated by extrapolating the gradient of the OCT velocity profiles to the pipe wall. In other words, instead of a direct measurement, the pressure loss can be obtained from the equation:

$$\Delta p_{OCT} = \pi D L \tau_{OCT} \quad (5)$$

where

$$\tau_{OCT} = \mu_{\text{water}} \left(\frac{dv(r)}{dr} \right)_{r \to R} \quad (6)$$

Given the shear stress at the wall, the friction factor f for water using the combination of volumetric flow and OCT measurements can be calculated as

$$f(\text{Re}) \equiv \frac{\Delta p}{\frac{L}{D}\frac{\rho V^2}{2}}, \text{Re} = \frac{\rho V D}{\mu} \quad (7)$$

Where Δp is the pressure loss, L is the pipe length, ρ is the fluid density, D is the pipe diameter, μ is the fluid viscosity, and Re is the Reynolds number.

In **Fig. 7**, the measured friction factor f is shown for the Reynolds number range of 70-10000 for water flowing in a straight tube with a circular cross-section and smooth walls.

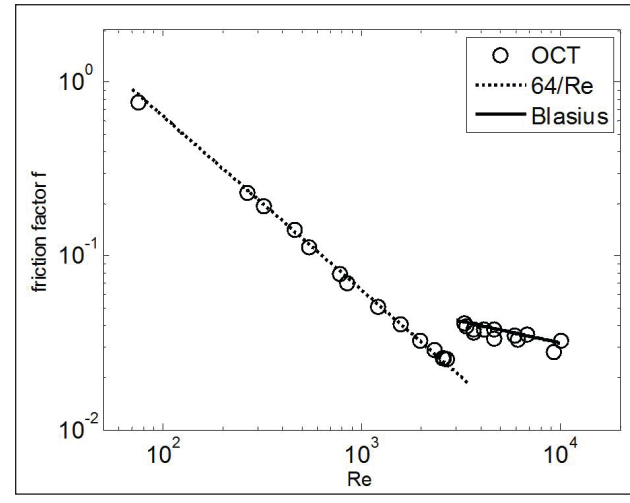

7. The friction factor of pipe flow measured with optical coherence tomography for water. The dashed line shows the theoretical prediction for the laminar region, and the solid line is the prediction for turbulent flow given by the Blasius equation.

The results are seen to correlate very well with the theoretical predictions [25].

Velocity profile and structure of MFC in pipe flow

After the verification measurements, the system was used for measuring the rheological properties of MFC suspensions. **Figure 8** shows an example of the combined mean velocity

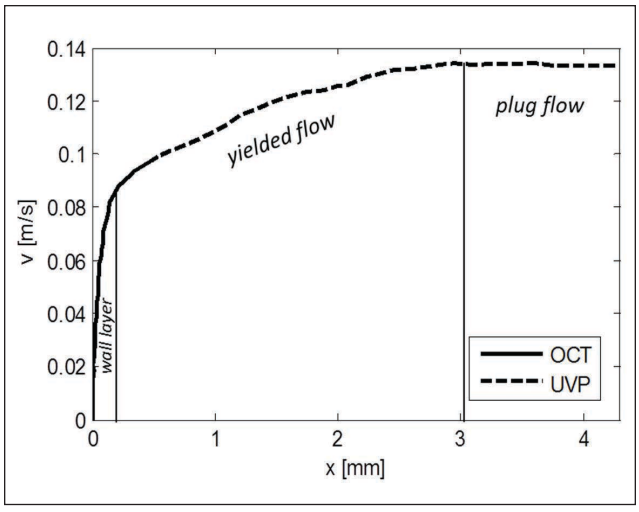

8. The velocity profile for a pipe flow (diameter 8.6 mm) of 0.4% MFC measured simultaneously by OCT and UVP.

profiles for 0.4% MFC in a pipe with diameter of 8.6 mm. UVP data from very close to the pipe wall have been omitted from the profile because of the known measurement limitations [5]. The agreement between the OCT and UVP velocity profiles is excellent, as with water, but now the spatial measurement range of the two measurements is overlapping. The combined profile shows three different flow regions: plug flow, yielded flow, and a wall layer. In this case, the thickness of the wall layer is approximately 200 μm and more than 60% of the maximum velocity is reached within that distance. Any traditional measurement technique would fail to measure the wall layer and it would be interpreted as a wall slip of 60%.

The effective concentration fields of suspensions can be obtained from the back-scattering intensity measured by OCT. The origin of the apparent wall slip can now be seen in **Figs. 9** and **10**. In Fig. 9 we see a 3-dimensional OCT image of non-flowing 0.4% MFC suspension in the pipe. The image was taken instantly after the flow was stopped. A fiber-poor layer is clearly visible close to the pipe wall (dark areas).

Figure 10 shows an instantaneous and an average concentration OCT image of MFC suspension flowing near the tube wall. The OCT images are constructed as the spatial distribution of the back-scattering index of light which, in turn, correlates with the concentration of the scattering particles. The scattering intensity profile (effective concentration) and the velocity profile are overlaid with the grayscale images. The concentration profile shows an approximately 200 μm thick layer of increasing concentration close to the wall. The existence of a wall concentration profile indicates that the fluid viscosity must change with the distance from the wall. There is a large variation in the velocity gradient close to the wall, although the shear stress is practically constant in such a narrow area. The viscosity profile calculated from Eq. (2) is shown in Fig. 10b. It shows that, near the wall, the viscosity is very close to that of water. This suggests that in the vicinity of the wall, there is a layer of almost pure water. The viscosity increases exponentially until it saturates to its bulk value at approximately 200 μm from the wall. To our knowledge, these are the first examples on such detailed experimental data on the fiber suspension properties very close to the wall.

Figure 11a shows the viscosity of the 0.4% suspension at the wall as a function of the wall shear stress. The wall viscosity decreases with increasing wall shear stress and

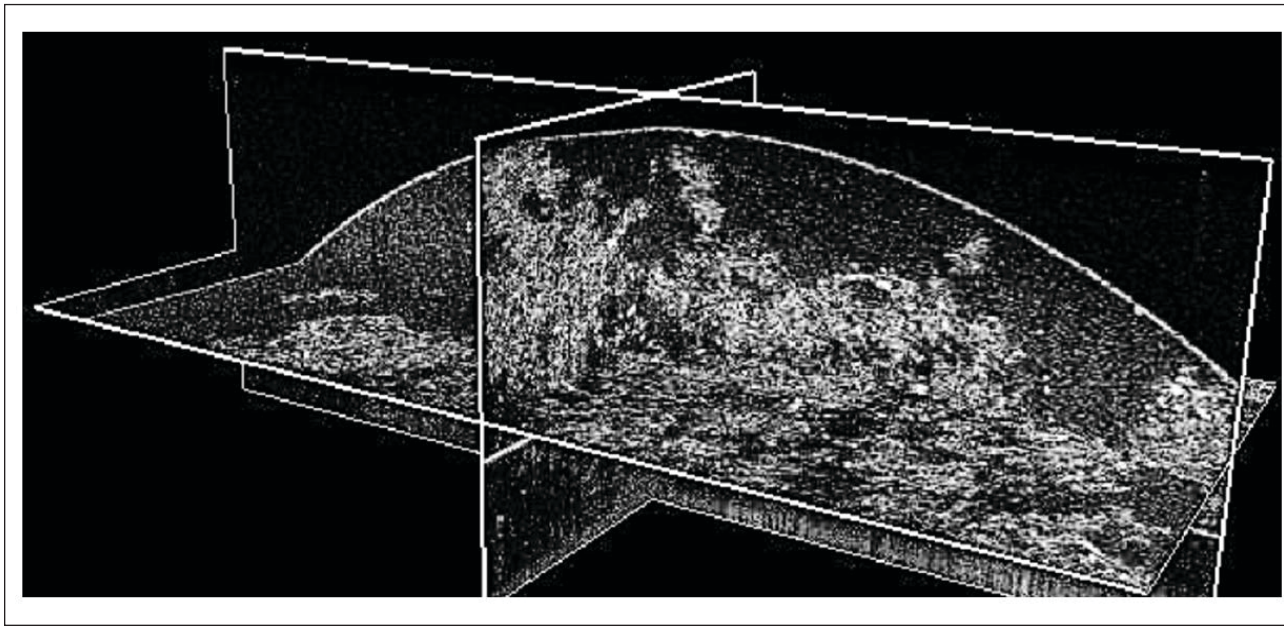

9. A 3-dimensional OCT image of 0.4% MFC in a pipe with a diameter of 8.6 mm. An almost fiber-free layer (black areas) is clearly visible close to the pipe walls.

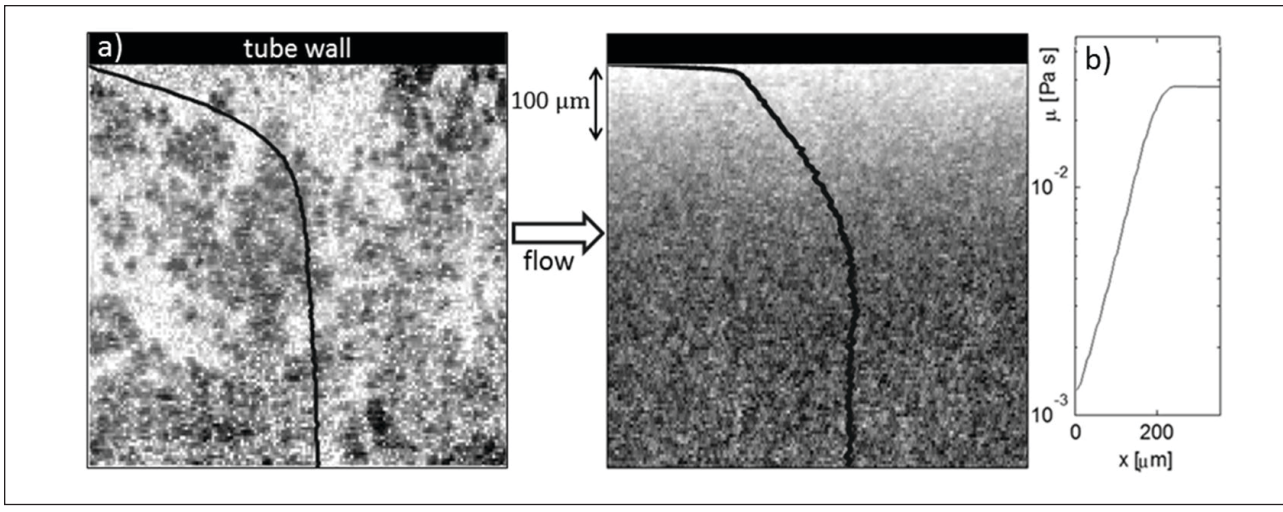

10. A 0.4% MFC suspension flowing near the tube wall. On the left an instantaneous image and on the right an average of 200 independent images acquired with the OCT techniques are shown. The grey-scale values in the image represent the local value of the optical back-scattering index, light color corresponding to low index value. The velocity profile and the scattering intensity (effective concentration) of the suspension are shown with black curves. On the right the viscosity profile close to the wall is shown.

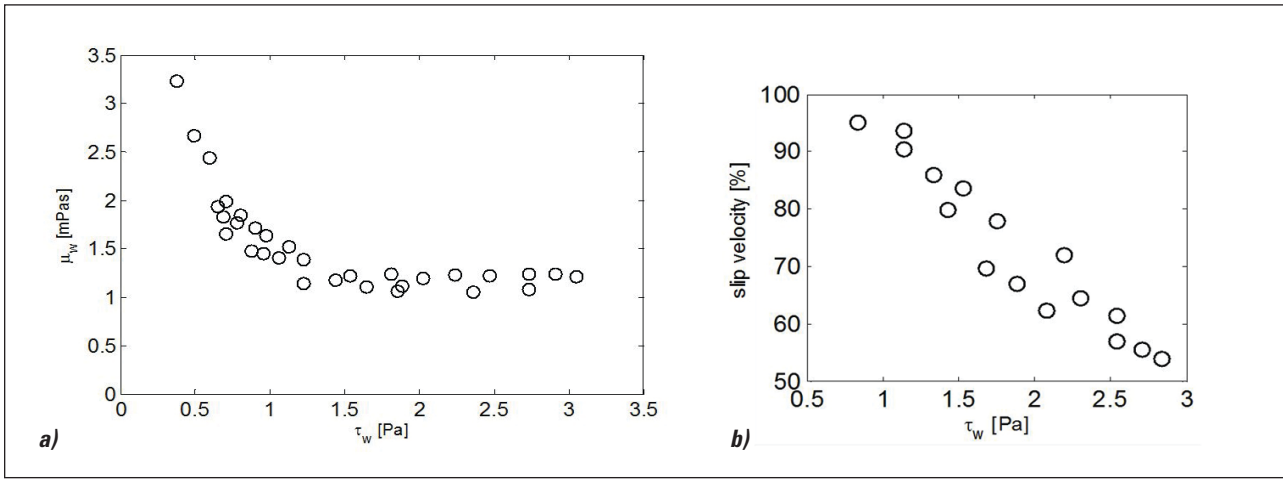

11. (a) The viscosity μ_w of the 0.4% MFC suspension at the wall as the function of wall shear stress τ_w. The wall viscosity decreases with increasing wall shear stress and saturates to $\mu_w \sim 1.2\ \mu_{water}$ when $\tau_w \sim 2\tau_y$ (approximately twice the yield stress; see Fig. 1b). (b) The contribution of slip velocity to the total volumetric flow as a function of the wall shear stress for 0.4% MFC.

saturates to a 20% higher value than the viscosity of water when the wall shear stress is approximately twice the yield stress. Similar behavior is observed for the consistencies of 1.0% and 1.7% (**Fig. 12**). In Fig. 11b, the contribution of the slip velocity to the total volumetric flow is shown as the function of the wall shear stress for 0.4% MFC. The slip velocity completely dominates the flow with the smallest wall shear rates and appears to decrease linearly when the wall shear stress increases. Salmela et al. provide a more careful analysis of the wall layer [8].

Rotational rheometer

Figure 13 shows the flow curves for a 1% MFC suspension. MFC suspensions typically show strong shear thinning behavior and flow curves often include a plateau between the low and high shear rate regions. This region, called the transition region or Newtonian plateau, is well known and reported for MFC [16-20]. The Newtonian plateau has been observed with different measuring geometries, including plate-and-plate [19,20] and concentric cylinders [16] geometries. Although not thoroughly researched, the reason for the transition at intermediate shear rates has been proposed to be the result of structural changes [19,20]. In this section, we aim to bring more insight on interpreting the rheometer data using OCT measurements.

Low shear rate and transition regions

Figure 14 shows the suspension structure and velocity profiles at three different apparent shear rates. Here, the velocity profiles were determined by tracking the horizontal

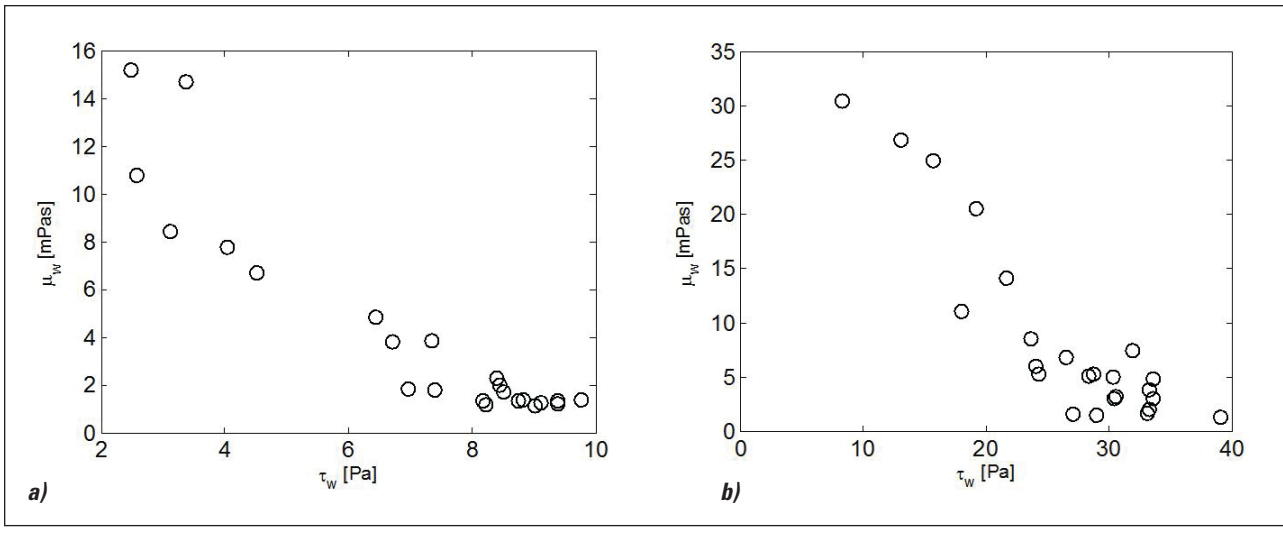

12. (a) The viscosity μ_w of the 1.0% MFC suspension at the wall as the function of wall shear stress τ_w. The wall viscosity decreases with increasing wall shear stress and saturates to $\mu_w \sim 2\,\mu_{water}$ when $\tau_w \sim 2\tau_y$ (approximately twice the yield stress). (b) The viscosity μ_w of the 1.7% MFC suspension at the wall as the function of wall shear stress τ_w. The wall viscosity decreases with increasing wall shear stress and appears to saturate when $\tau_w \sim 2\tau_y$.

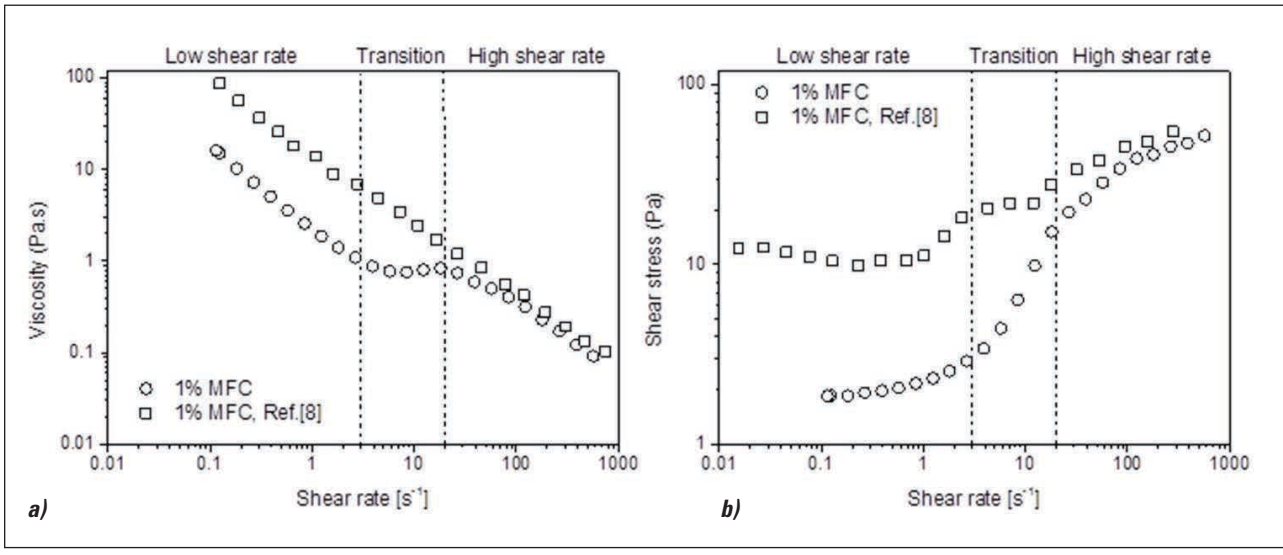

13. Viscosity and shear stress as a function of apparent shear rate for 1% MFC suspension. The viscosity is calculated assuming an ideal (linear) velocity profile in the rheometer gap. Lavoine et al. [16] preformed measurements after pre-shearing from low shear rates to high shear rates.

displacement of the MFC flocs between sequential structure images using an optical flow algorithm [21]. Results show that the fibers are not evenly distributed in the gap, and the velocity profile is not linearly decreasing to zero toward the outer wall, as is normally assumed when calculating the viscosity. So, despite looking reasonable, the flow curve cannot be used for analyzing the bulk properties of MFC — at least not in this flow region. It would be very difficult to make such a conclusion using the rheometer data alone. However, analysis of the values of shear stress can in many cases help here. We have found that for MFC with concentrations of 0.1%-2%, the shear stress is often approximately constant or increases very slowly in the low shear rate region [16,21]. The (wall) shear stress is then almost independent of the rotation speed of the inner cylinder. This strongly indicates that the rheometer data might be dominated by boundary layer phenomena, not by the bulk properties of MFC. This has been discussed in more detail by Saarikoski et al. [21].

The MFC viscosity (μ) is often characterized with the power law model:

$$\mu = K\dot{\gamma}^{n-1} \tag{9}$$

where K is the consistency index and n is the flow index. If

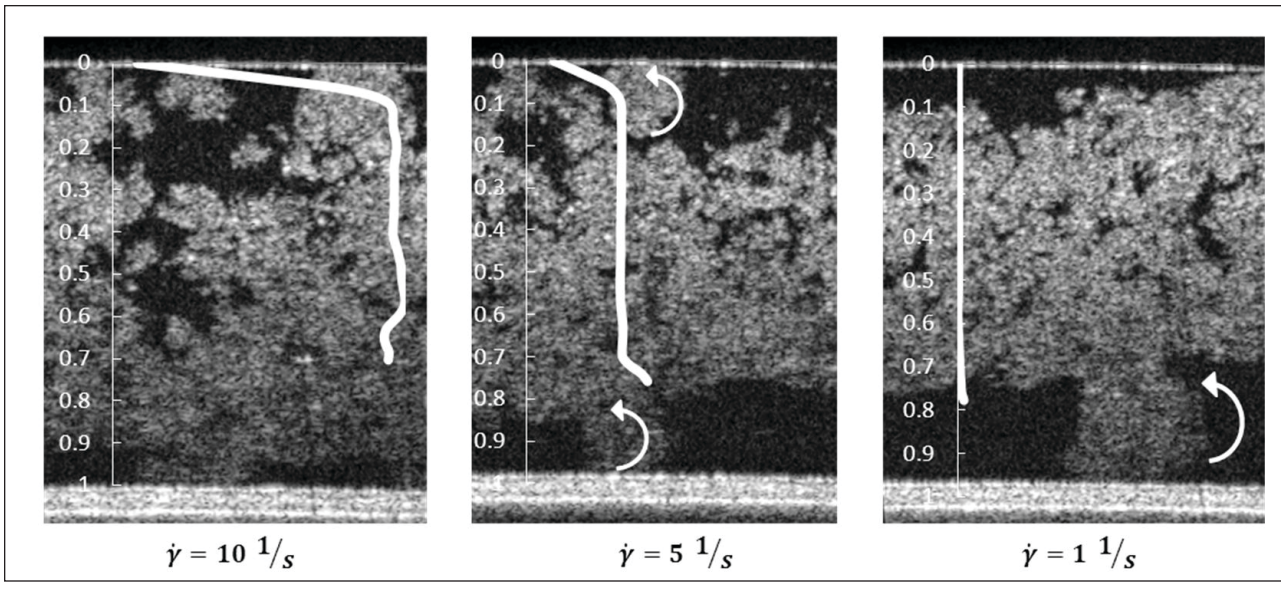

14. Different flow regimes for 1% MFC in a cylindrical rotational rheometer: (a) Complete slip on the stationary wall. (b) Slip and rolling flocs on both walls. (c) Rolling flocs on the moving wall. The gap is 1.0 mm. The average velocity profiles are marked with a white line.

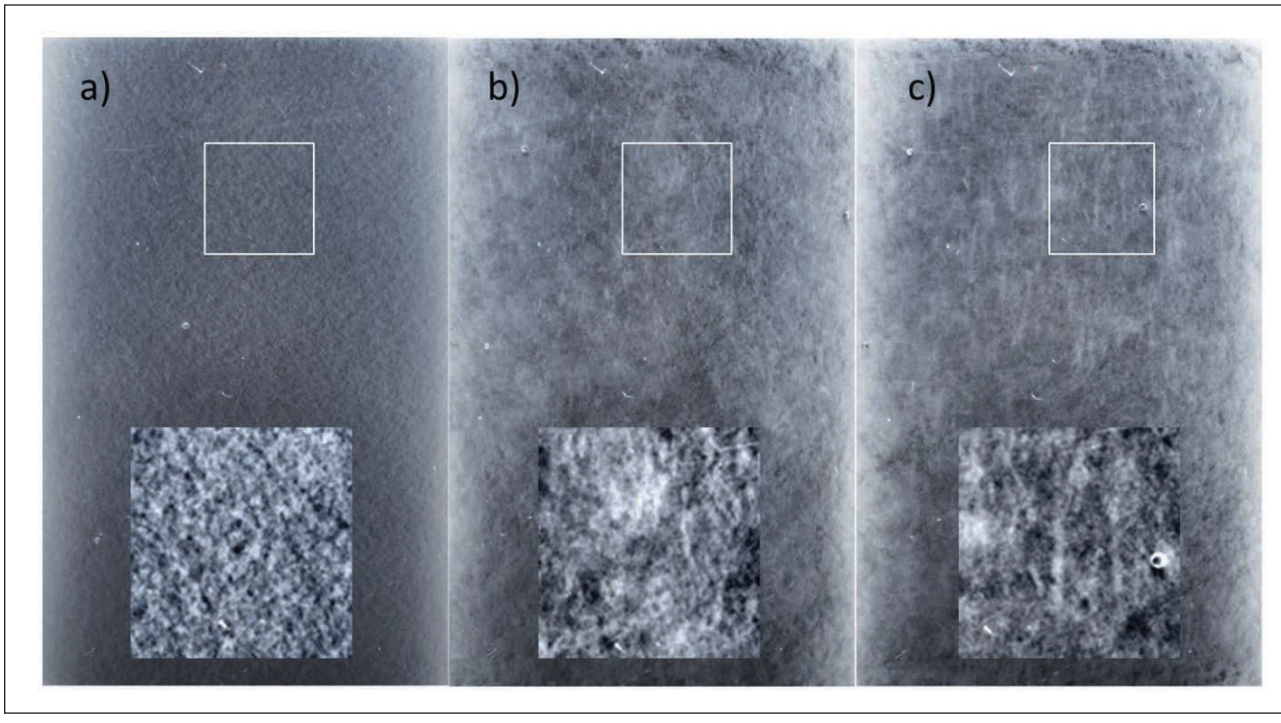

15. MFC suspensions in the rheometer gap at different shear rates: (a) 108 s^{-1}, (b) 11 s^{-1}, and (c) 1 s^{-1}.

the shear stress is almost constant, the flow index n is close to 0. It seems that flow index values smaller than ~0.2 with the rheometer data are less reliable [15]. This is also the case in Fig. 13, where n gets values 0.0 and 0.16 in the low shear rate region.

Figure 15 shows floc structures for 1% MFC suspension during the flow curve measurements photographed through the transparent outer cylinder. The photographs depict three different regions, showing that at high shear rates, the flocs are small and homogeneous. During the transition region (Fig. 15b), the separate flocs start to attach to each other in the decelerating flow, because the shearing is not sufficient to break the larger flocs. In our earlier study [16], we saw similar structures with increasing shear rate curve, meaning that the continuous network is breaking in the transition region. At the low shear rate region, the structure remains uneven and co-

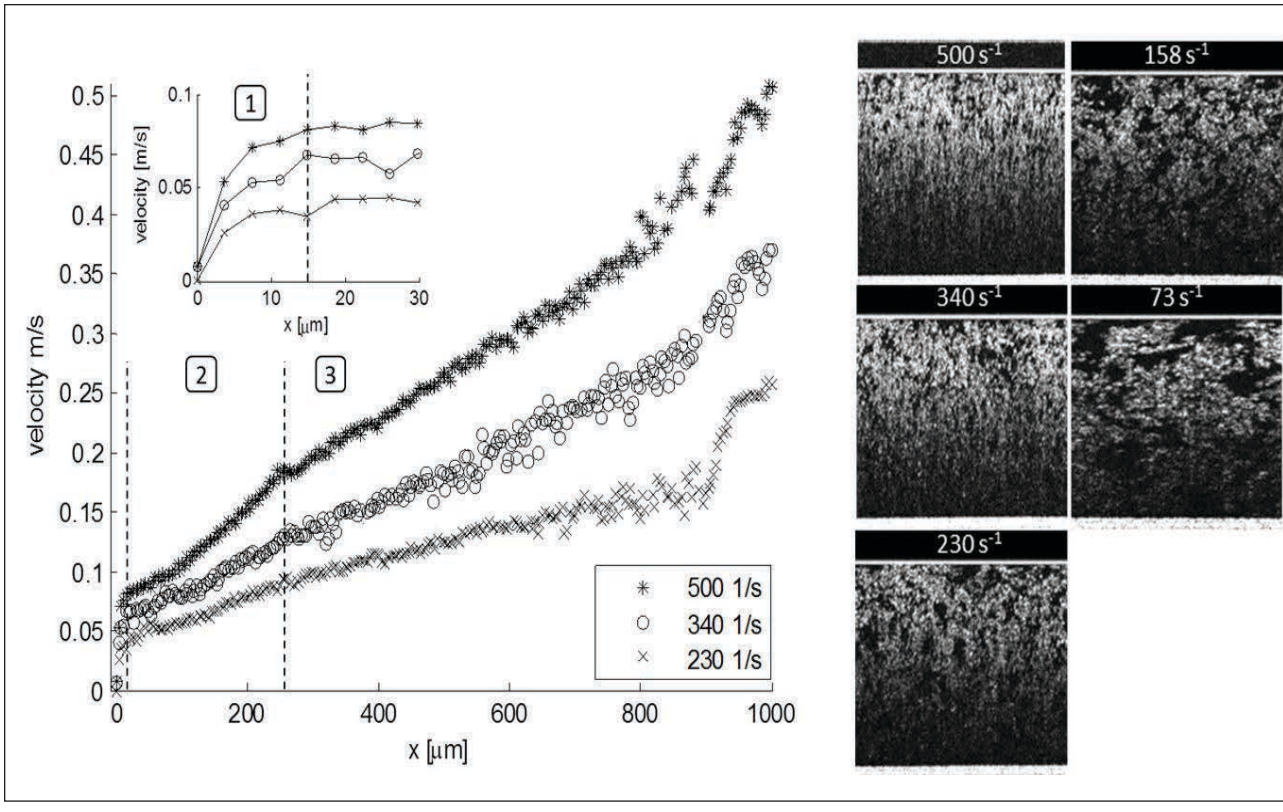

16. Velocity profiles and structure images in the high shear rate region. The profiles have three regions: (1) the wall slip layer, which is about 15 µm thick; (2) the wall boundary layer, which is about 250 µm thick, where the slope of the velocity profile is higher than in the middle of the gap; and (3) the middle area, where the shear rates are 55%-70% smaller than the apparent shear rate. (Note that the optical coherence tomography profiles close to the moving boundary are distorted and thus untrustworthy, probably because the intensity of the scattering signal becomes too small.)

herent, cylindrical, and rotating floc structures (rollers) emerge between the fiber network and the rotating cylinder. OCT results show the same rollers (Fig. 14).

High shear rate region

We see from Fig. 15a that the suspension is rather homogeneous when the shear rate is higher than 100 s^{-1}. **Figure 16** shows OCT velocity profiles and structure images with shear rates greater than 70 s^{-1}. The profiles have three regions:

1) The wall slip layer, which is about 15 μm thick. Near the wall, the viscosity of the suspension is close to water.

2) The wall boundary layer, where the slope of the velocity profile is higher than in the middle of the gap. This layer is about 250 μm thick.

3) The middle area, where the shear rates are 55%-70% smaller than the apparent shear rate. The velocity profiles still differ from the ideal, but in this region the bulk of the suspension exhibits true shear flow.

SUMMARY

Cellulose fiber suspensions are a challenge for conventional rheometers because of their small dimensions and often questionable assumptions about the behavior of the fluid in the gap. Both of these are still obligatory for interpreting the measurements. One can instead use a pipe rheometer in combination with the UVP-PD concept, where the real flow behavior is used for the rheological analysis of the bulk properties of the suspension. However, the resolution of UVP is too low for studying near-wall phenomena, such as the lubrication layer, that are often very important for understanding real-life flows. To address this problem, we augmented the UVP-PD concept with OCT measurements. This enables us to measure bulk and the wall-layer behavior simultaneously.

After verifying the accuracy of the OCT measurements with water, we applied OCT for MFC flow in the pipe rheometer and in a traditional rheometer equipped with a cylinder geometry. We showed that in both cases the boundary layer dynamics play a key role. We also noticed that wall slippage could not be eliminated by using rough or grooved surfaces in the rheometer. Therefore, one has to be very careful with the interpretation of data obtained with traditional rheometers.

In this work, we focused on studying mechanically disintegrated MFC grades in relatively low consistencies. However, OCT opens new possibilities for measuring boundary layer properties for other opaque fluids, including different MFC grades, also in higher consistencies. Our results clearly demonstrate the benefits of having direct measurement of the ve-

locity profile inside the rheometer. OCT has the potential for significant breakthroughs in understanding the rheological properties of complex opaque fluids. By using this method, we have already obtained new information about flow instabilities inside a rheometer gap and used this data to interpret rheometer flow curve [27]. We have also been able to perform a thorough study of the behavior and dynamics of the MFC wall layer during its pipe flow [8].

ACKNOWLEDGEMENTS

We gratefully acknowledge the valuable co-operation network of COST ACTION FP 1005 (Fibre Suspension Flow Modelling) and ERCOFTAG SIG 43 (Fibre Suspension Flows). We also gratefully acknowledge the Academy of Finland (project Rheological Properties of Complex Fluids) for supporting this work. In addition, "Efficient Networking Towards Novel Products and Processes" (EffNet) research program of Forestcluster Ltd. funded by Tekes — the Finnish Funding Agency for Technology and Innovation — and Forestcluster Ltd. is acknowledged. **TJ**

LITERATURE CITED

1. Haavisto, S., Lille, M., Liukkonen, J., et al., "Laboratory-scale pipe rheometry: a study of a microfibrillated cellulose suspension," *PaperCon*, TAPPI PRESS, Atlanta, GA, USA, 2011.
2. Ouriev, B. and Windhab, E.J., *Exp. Fluids* 32(2): 204(2002).
3. Ouriev, B., Windhab, E.J., Braun, P., et al., *Rev. Sci. Instrum.* 75(10): 3164(2004).
4. Dogan, N., McCarthy, M.J., and Powell, R.L., *Meas. Sci. Technol.* 16(8): 1684(2005).
5. Wiklund, J. and Stading, M., *Flow Meas. Instrum.* 19(3-4): 171(2008).
6. Steger, R., "Optisch und Akustische Methoden in Der Rheometrie," Dissertation, Friedrich-Alexander-Universität, Erlangen-Nürnberg, Germany, 1994.
7. Müller, M., Brunn, P.O., and Wunderlich, T., *Appl. Rheol.* 7(5): 204(1997).
8. Salmela, J., Haavisto, S., Koponen, A., et al., *Fundam. Res. Symp., 15th*, The Pulp and Paper Fundamental Research Society, Bury, Lancashire, UK, 2013, p. 405.
9. Jäsberg, A., "Flow behavior of fiber suspensions in straight pipes: new experimental techniques and multiphase modelling", Ph.D. thesis, University of Jyväskylä, Jyväskylä, Finland, 2007.

ABOUT THE AUTHORS

Cellulose fiber suspensions are a challenge for conventional rheometers due to their small dimensions and due to often-questionable assumptions of the behavior of the fluid in the rheometer gap. Due to recent research activity with microfibrillated (MFC) and nanofibrillated (NFC) celluloses, these difficulties have been addressed repeatedly, resulting in indirect evidence of intricate flow phenomena, such as instability, flocculation, and wall slip inside a rotational rheometer.

The restrictions imposed by the measurement system size can be avoided by using pipe rheometers based on, e.g., the ultrasound velocity profiling -pressure difference (UVP-PD) concept. However, these methods most likely provide only the bulk behavior of the fluid because the velocity measurement resolution is too limited to detect near-wall phenomena. With our extensive background in rheology, as well as our knowledge in fiber suspension flows, we explored the flow phenomena of MFC suspensions both inside a rheometer and in a pipe rheometer.

The most challenging aspects of this work were to achieve correct measurement setup and conditions to enable accurate measurements that enable the simultaneous interpretation of both the bulk and the wall-layer behavior. In earlier studies, optical coherence tomography (OCT) has mainly been applied in biomedical flows where the channel dimensions have been very small. As a result of this work, we discovered that boundary layer dynamics play a key role both in the pipe flow and in the traditional rheometer. The measurements can be continued further to get information on the complex processes taking place in the wall layer. This information would be invaluable in flow control and numerical simulations of (MFC) fiber suspension flows.

Haavisto is R&D engineer and Salmela is CTO, Spinnova Ltd., Jyväskylä, Finland. Jäsberg is senior scientist and Koponen is principal investigator, VTT, Technical Research Centre of Finland, Jyväskylä, Finland. Saarinen is product manager, Betulium Ltd., Espoo, Finland. Karppinen is researcher at Borregaard, Sarpsborg, Norway. Email Koponen at antti.koponen@vtt.fi.


Haavisto


Salmela


Jäsberg


Saarinen


Karppinen


Koponen

10. Chow, A., Sinton, S., and Iwamiya, J., *Phys. Fluids* 6(8): 2561(1994).
11. Takeda, Y., *Exp. Therm. Fluid Sci.* 10(4): 444(1995).
12. Harvey, M. and Waigh, T.A., *Phys. Rev. E: Stat., Nonlinear, Soft Matter Phys.* 83(3 Pt 1): 031502(2011).
13. Haavisto, S., Koponen, A., Salmela, *J., Front. Chem.* 2: 27(2014).
14. Haavisto, S., Salmela, J., Koponen, A., *Exp. Fluids* 56(5): 1(2015).
15. Haavisto, S., Salmela, J., Jäsberg, A., et al., *PaperCon*, TAPPI PRESS, Atlanta, GA, USA, 2013, p. 1119.
16. Lavoine, N., Desloges, I., Dufresne, A., et al., *Carbohydr. Polym.* 90(2): 735(2012).
17. Lowys, M., Desbrières, J., and Rinaudo, M., *Food Hydrocolloids* 15(1): 25(2001).
18. Pääkkö, M., Ankerfors, M., Kosonen, H., et al., *Biomacromolecules* 8(6): 1934(2007).
19. Agoda-Tandjawa, G., Durand, S., Berot, S., et al., *Carbohydr. Polym.* 80(3): 677(2010).
20. Iotti, M., Gregersen, O.W., Moe, S., et al., *J. Polym. Environ.* 19(1): 137(2011).
21. Saarikoski, E., Saarinen, T., Salmela, J., et al., *Cellulose* 19(3): 647(2012).
22. Karppinen, A., Saarinen, T., Salmela, J., et al., *Cellulose* 19(6): 1807(2012).
23. Kasai, C., Namekawa, K., Koyano, A., et al., *IEEE Trans. Sonics Ultrason.* 32(3): 458(1985).
24. Tatsumi, D., Ishioka, S., and Matsumoto, T., *J. Soc. Rheol., Jpn.* 32(1): 27(2002).
25. White, F.M., *Fluid Mechanics*, 3rd edn., McGraw-Hill Education, New York, 1994, pp. 310-315.
26. Spalding, D.B., *J. Appl. Mech.*, 28(3): 455(1961).
27. Saarinen, T., Haavisto, S., Sorvari, A., et al., *Cellulose* 21(3): 1261(2014).